ORIGINAL RESEARCH

eNAMPT Is a Novel Damage-associated Molecular Pattern Protein That Contributes to the Severity of Radiation-induced Lung Fibrosis

Alexander N. Garcia[1]*, Nancy G. Casanova[2]*, Carrie L. Kempf[2]*, Tadeo Bermudez[2], Daniel G. Valera[2], Jin H. Song[2], Xiaoguang Sun[2], Hua Cai[3], Liliana Moreno-Vinasco[2], Taylor Gregory[2], Radu C. Oita[2], Vivian Reyes Hernon[2], Sara M. Camp[2], Claude Rogers[4], Espoir M. Kyubwa[4], Naresh Menon[4], James Axtelle[4], Jay Rappaport[5], Christian Bime[2], Saad Sammani[2], Anne E. Cress[6], and Joe G. N. Garcia[2]

[1]Department of Radiation Oncology, [2]Department of Medicine, and [6]Department of Cell and Molecular Medicine, University of Arizona Health Sciences, Tucson, Arizona; [3]Department of Anesthesiology, University of California Los Angeles, Los Angeles, California; [4]ChromoLogic LLC, Monrovia, California; and [5]Tulane National Primate Research Center, New Orleans, Louisiana

ORCID IDs: 0000-0002-6363-2414 (N.G.C.); 0000-0003-4450-4510 (D.G.V.); 0000-0002-0123-2909 (J.H.S.); 0000-0003-4226-8294 (X.S.); 0000-0001-5521-9841 (S.M.C.); 0000-0003-1359-6280 (N.M.); 0000-0003-4787-2685 (C.B.); 0000-0002-7933-6388 (S.S.); 0000-0001-6194-0061 (A.E.C.); 0000-0002-6934-0420 (J.G.N.G.).

Abstract

The paucity of therapeutic strategies to reduce the severity of radiation-induced lung fibrosis (RILF), a life-threatening complication of intended or accidental ionizing radiation exposure, is a serious unmet need. We evaluated the contribution of eNAMPT (extracellular nicotinamide phosphoribosyltransferase), a damage-associated molecular pattern (DAMP) protein and TLR4 (Toll-like receptor 4) ligand, to the severity of whole-thorax lung irradiation (WTLI)-induced RILF. Wild-type (WT) and *Nampt*$^{+/-}$ heterozygous C57BL6 mice and nonhuman primates (NHPs, *Macaca mulatta*) were exposed to a single WTLI dose (9.8 or 10.7 Gy for NHPs, 20 Gy for mice). WT mice received IgG_1 (control) or an eNAMPT-neutralizing polyclonal or monoclonal antibody (mAb) intraperitoneally 4 hours after WTLI and weekly thereafter. At 8–12 weeks after WTLI, NAMPT expression was assessed by immunohistochemistry, biochemistry, and plasma biomarker studies. RILF severity was determined by BAL protein/cells, hematoxylin and eosin, and trichrome blue staining and soluble collagen assays. RNA sequencing and bioinformatic analyses identified differentially expressed lung tissue genes/pathways. NAMPT lung tissue expression was increased in both WTLI-exposed WT mice and NHPs. *Nampt*$^{+/-}$ mice and eNAMPT polyclonal antibody/mAb-treated mice exhibited significantly attenuated WTLI-mediated lung fibrosis with reduced: *1*) NAMPT and trichrome blue staining; *2*) dysregulated lung tissue expression of smooth muscle actin, p-SMAD2/p-SMAD1/5/9, TGF-β, TSP1 (thrombospondin-1), NOX4, IL-1β, and NRF2; *3*) plasma eNAMPT and IL-1β concentrations; and *4*) soluble collagen. Multiple WTLI-induced dysregulated differentially expressed lung tissue genes/pathways with known tissue fibrosis involvement were each rectified in mice receiving eNAMPT mAbs.The eNAMPT/TLR4 inflammatory network is essentially involved in radiation pathobiology, with eNAMPT neutralization an effective therapeutic strategy to reduce RILF severity.

Keywords: whole-lung thoracic irradiation; nicotinamide phosphoribosyltransferase; eNAMPT; TLR4; DAMP

Clinical Relevance

Preclinical lung irradiation studies support the role of inflammation in determining the severity of radiation-induced lung fibrosis (RILF) but have not yet successfully translated to a specific clinical therapy. We evaluated eNAMPT (extracellular nicotinamide phosphoribosyltransferase), a damage-associated molecular pattern (DAMP) protein and TLR4 (Toll-like receptor 4) ligand, in a preclinical RILF model. Targeting the eNAMPT/TLR4 pathway with a humanized eNAMPT-neutralizing mAb effectively reduced RILF severity, suggesting a potential therapeutic strategy to directly address an important medical and societal unmet need for patients undergoing cancer radiotherapy or with accidental exposure to ionizing radiation.

(Received in original form August 10, 2021; accepted in final form December 17, 2021)

*Co–first authors.

Supported by National Institutes of Health grants R01 HL094394 and R42 HL152888 and National Heart, Lung, and Blood Institute grant P01 HL134610.

Am J Respir Cell Mol Biol Vol 66, Iss 5, pp 497–509, May 2022

Originally Published in Press as DOI: 10.1165/rcmb.2021-0357OC on February 15, 2022
Internet address: www.atsjournals.org

The development of radiation-induced lung fibrosis (RILF) is a disabling, potentially fatal toxicity in patients with lung or esophageal cancer undergoing radiotherapy or individuals with accidental ionizing radiation (IR) exposure (1–4). Approximately 15% of patients with lung cancer develop RILF after radiotherapy (5), with radiation dose/hypofractionation, dose-rate fraction size, volume of lung irradiated, time course of treatment delivery, comorbid factors (e.g., emphysema), genetic factors, and concurrent chemotherapy all serving as important RILF-determining variables (2). RILF is often progressive, with current therapeutic interventions neither halting nor reversing the fibrotic process and only weakly slowing RILF progression. Preclinical and clinical trials examining multiple RILF therapeutics have shown only very modest improvement (6–10). Multiple studies of prophylactic steroid administration, the cornerstone of standard therapy for radiation pneumonitis, found little benefit in RILF (3, 11). Thus, despite ongoing efforts, effective therapeutic mitigators for RILF do not currently exist, highlighting a serious unmet medical and societal need for effective medical countermeasures.

The pathobiology of RILF is complex but involves IR-stimulated activation of evolutionary conserved inflammatory pathways, including pathogen-recognition receptors such as the Toll-like receptor (TLR) family (12, 13). IR-mediated inflammation elicits increased leukocyte infiltration, increased permeability of lung endothelial and epithelial barriers, and increases in circulating concentrations of multiple inflammatory cytokines and growth factors, events implicated in both the development and severity of radiation injury (14, 15). In addition, IR-stimulated inflammation is a key contributor to fibrogenesis (1, 15, 16), fibroblast conversion to myofibroblasts, and excess deposition of collagen and other extracellular matrix components. Experimental/clinical therapies that neutralize proinflammatory cytokines as a strategy to ameliorate IR-induced RILF have, unfortunately, been disappointing (3). Effective antiinflammatory strategies to reduce RILF occurrence and severity are a continued unmet need.

We previously used preclinical murine whole-thorax lung irradiation (WTLI) models to explore the role of inflammation in driving the severity of radiation pneumonitis and RILF and to evaluate potential biomarkers (17), druggable pathways (18), and therapeutic strategies (8, 16, 19, 20). Our genomic studies highlighted the role of inflammation and TLR signaling (19, 20). As damage-associated molecular pattern (DAMP) molecules play a vital role in promoting both progression of pulmonary fibrosis (21, 22) and the response to radiation exposure (1), our recent preclinical RILI studies have focused on the role of eNAMPT (extracellular nicotinamide phosphoribosyltransferase), a novel DAMP and regulator of innate immunity inflammation, as a potential therapeutic inflammatory target in IR-induced injury (23–25). eNAMPT binds to the pathogen-recognition receptor TLR4 (14, 26) and serves as a novel therapeutic target in acute respiratory distress syndrome (ARDS)/ventilator-induced lung injury (14, 24, 25, 27–29), pulmonary arterial hypertension (PAH) (30, 31), prostate cancer (32), and inflammatory bowel disease (33). We recently demonstrated that NAMPT expression in human lung epithelium and in murine lung tissues is increased by radiation exposure (23). eNAMPT neutralization with a humanized monoclonal antibody (mAb) significantly reduced the severity of murine radiation-induced inflammatory lung injury, with genomic and biochemical studies highlighting dysregulation of the TLR4/NF-κB, IL-1β, and MAP kinase signaling pathways (23).

The current studies were designed to explore the hypothesis that the novel DAMP, eNAMPT, is an important contributor to not only radiation pneumonitis, an early complication of IR exposure, but also the development of RILF, a delayed life-threatening pathobiology. Marked increases in eNAMPT lung tissue expression were identified in WTLI-exposed nonhuman primates (NHPs) and mice with lung fibrosis. A humanized eNAMPT-neutralizing mAb demonstrated the eNAMPT/TLR4 signaling is essentially involved in radiation pathobiology. eNAMPT mAb neutralization was an effective therapeutic strategy to reduce RILF severity, dysregulate the master fibrosis-regulatory TGF-β/SMAD pathway, reduce expression of the reactive oxygen species (ROS)-generating NOX4, and restore expression of the key antioxidant transcription factor NRF2. RNA sequencing (RNAseq) of WTLI lung tissues corroborated lung tissue proteomic studies and revealed multiple differentially expressed genes (DEGs) and signaling pathways with known involvement in tissue fibrosis. These studies suggest that a preventive eNAMPT-neutralizing strategy may directly address the unmet medical and societal needs associated with IR exposure.

Methods

Reagents

Unless otherwise noted in the online supplement, reagents were purchased from Sigma-Aldrich. Details of the eNAMPT-neutralizing polyclonal antibody (pAb) and humanized mAb (ALT-100 mAb, Aqualung Therapeutics) have been previously reported (23–25).

Whole Thoracic Lung Irradiation

Murine studies. Experiments used either wild-type (WT) male C57BL/6J mice (20–25 g, 8–12 wk), or *Nampt*$^{+/-}$ heterozygous mice generated as we previously described (23, 24, 30) (*see* online supplement). WT and *Nampt*$^{+/-}$ heterozygous mice or littermate control mice were exposed to WTLI

Author Contributions: A.N.G., N.G.C., A.E.C., and J.G.N.G.: Conception and design of the work, analysis and interpretation of data for the work, drafting and revision of the manuscript, critical revision of key intellectual content, and approval of final version to be published. A.N.G., C.L.K., T.B., D.G.V., J.H.S., X.S., H.C., L.M.-V., T.G., R.C.O., V.R.H., S.M.C., C.R., E.M.K., N.M., J.A., J.R., C.B., and S.S.: Collection of data and assistance with processing and manuscript revision.

Correspondence and requests for reprints should be addressed to Joe G. N. Garcia, M.D., University of Arizona Health Sciences, 1230 North Cherry Avenue, Room 441, Tucson, AZ 85721. E-mail: skipgarcia@email.arizona.edu.

This article has a related editorial.

This article has a data supplement, which is accessible from this issue's table of contents at www.atsjournals.org.

radiation (20 Gy) as described previously (8, 20, 23) (online supplement).

NHP studies. Blood and tissues were obtained from *Macaca mulatta* control animals and animals randomly assigned to receive WTLI 9.8 Gy (six males, six females) or 10.7 Gy (LD75/180; eight males, eight females). Before WTLI, animals were anesthetized with ketamine/xylazine and restrained on the linear accelerator (LINAC) couch. Radiation was delivered using a 6-MV photon source LINAC (0.60 ± 0.10 Gy/min, Varian CLINAC 21EX, Varian Associates) with ~50% dose contribution from anterior-posterior and posterior-anterior beams (34, 35).

BAL Analysis

BAL for protein analysis and cell count was performed as previously described (23, 25) (online supplement).

Quantitative Lung Histology and Immunohistochemistry Staining

Lungs were fixed and processed for hematoxylin and eosin or immunohistochemistry (IHC) staining for NAMPT as previously described (23, 25). Representative images were selected for quantification using ImageJ software as described previously (25) (online supplement).

Biochemical Analyses of Murine Lung Tissues

Lung tissue homogenates were used for Western blotting as previously described (23, 25), with densitometric quantification with β-actin normalization (online supplement).

Sircol Soluble Collagen Assay

The collagen content in murine lung tissues was determined by Sircol Collagen Assay kit (Biocolor). Total protein assay (Bio-Rad Laboratories) was used as control to normalize collagen content of each sample (36).

Plasma Cytokine Measurements

Plasma biomarkers were measured in 20-Gy–exposed mice (eNAMPT, IL-1β) and 10.7-Gy–exposed NHPs (IL-6, IL-1RA, MIF, Ang-2) using a mesoscale ELISA platform (Meso Scale Diagnostics) as previously described (23, 25) (online supplement).

Lung Tissue RNASeq Analysis

Total RNA extracted from lung tissues as previously described (20, 23) was sequenced using the BGISEQ platform and analyzed as described in the online supplement. A false discovery rate of 0.05 was applied to identify significantly enriched pathways using Gene Ontology (GO) classification, Kyoto Encyclopedia of Genes and Genomes (KEGG) (37) and Reactome (13, 38) Databases . The STRING (39) database was utilized to analyze protein and protein interactions.

microRNA Analysis in NHPs

Plasma microRNA (miRNA) was isolated using the miRNEasy Serum/Plasma Advanced Kit (Qiagen) and next-generation sequencing (NextSeq 550, Illumina) performed as described in the online supplement. miRTarBase and miRWalk softwares, with predicted and validated miRNA interactions mRNA transcripts, were used to identify miRNAs binding the *NAMPT* 3′ untranslated region (UTR) (40). KEGG pathways associated with differentially expressed miRNAs were identified using mirPath v.3 software (online supplement).

Statistical Analysis

Means of data from two or more different experimental groups were compared using two-way ANOVA. Differences between groups were considered statistically significant when $P < 0.05$. If significant difference was present by ANOVA ($P < 0.05$), a least significant differences test was performed *post hoc*.

Results

Thoracic Irradiation Exposure Increases NAMPT Lung Tissue Expression and Lung Fibrosis in Mice and NHPs

Histologic and IHC studies were designed to assess murine and NHP lung tissue responses to thoracic irradiation. Compared with control animals (inset), representative images from both WTLI-exposed mice (20 Gy, 12 wk) and NHPs (10.7 Gy, 9 wk) exhibited significant hematoxylin and eosin evidence of lung inflammation and alveolar wall thickening (Figures 1A and 1D), which was accompanied by marked increases in NAMPT lung tissue expression (Figures 1B and 1E), findings supported by increased lung NAMPT immunoreactivity/expression in WTLI-exposed lung homogenates (*see* Figure E1 in the online supplement). The presence of WTLI-induced lung fibrosis in both WTLI-exposed mice and NHPs was demonstrated by the significant increase in trichrome blue staining in lung tissues (Figures 1C and 1F), reflecting increased collagen deposition, a finding similar to the extent of RILF we previously observed at this degree of IR exposure (8, 16–20).

eNAMPT Neutralization Reduces the Severity of Preclinical Radiation-induced Lung Inflammation and Fibrosis

To explore eNAMPT as a direct participant in RILF pathobiology, we assessed the efficacy of eNAMPT neutralization using either a pAb or humanized mAb, strategies previously shown to ameliorate inflammatory injury in preclinical models of ARDS (24, 25), pulmonary hypertension (31), prostate cancer (32), and, more recently, radiation pneumonitis (23). Intraperitoneal delivery of either the eNAMPT pAb or mAb, beginning within hours of 20-Gy exposure and continuing weekly thereafter, significantly reduced WTLI-mediated histologic evidence of inflammation cell infiltration and injury, quantified by ImageJ software analysis (Figures 2A and 2B), as well as the WTLI-induced increases in the extent of trichrome staining at 12 weeks reflecting significant reductions in RILF severity (Figures 2C and 2D). In addition, eNAMPT mAb-mediated reductions in RILF severity were corroborated by measurements of WTLI-induced weight loss (Figure E4) and lung tissue concentrations of soluble collagen (Figures 2E and 2F).

Consistent with the contribution of inflammatory pathways to the development of RILF, WTLI exposure significantly increased two BAL indices of inflammation, total BAL protein concentrations and cells (Figures 2G and 2H), with both indices significantly reduced in mice receiving eNAMPT-neutralizing antibodies (eNAMPT mAb and pAb). This was further confirmed by mAb-induced reductions in plasma concentrations of the inflammatory markers eNAMPT and IL-1β (Figures 2I and 2J). Similar to WTLI-exposed mice, WTLI-challenged NHPs demonstrated temporal alterations in plasma concentrations of inflammatory biomarkers IL-6, MIF, IL-1RA, and Ang-2 measured 60 days after WTLI exposure (Figure E2).

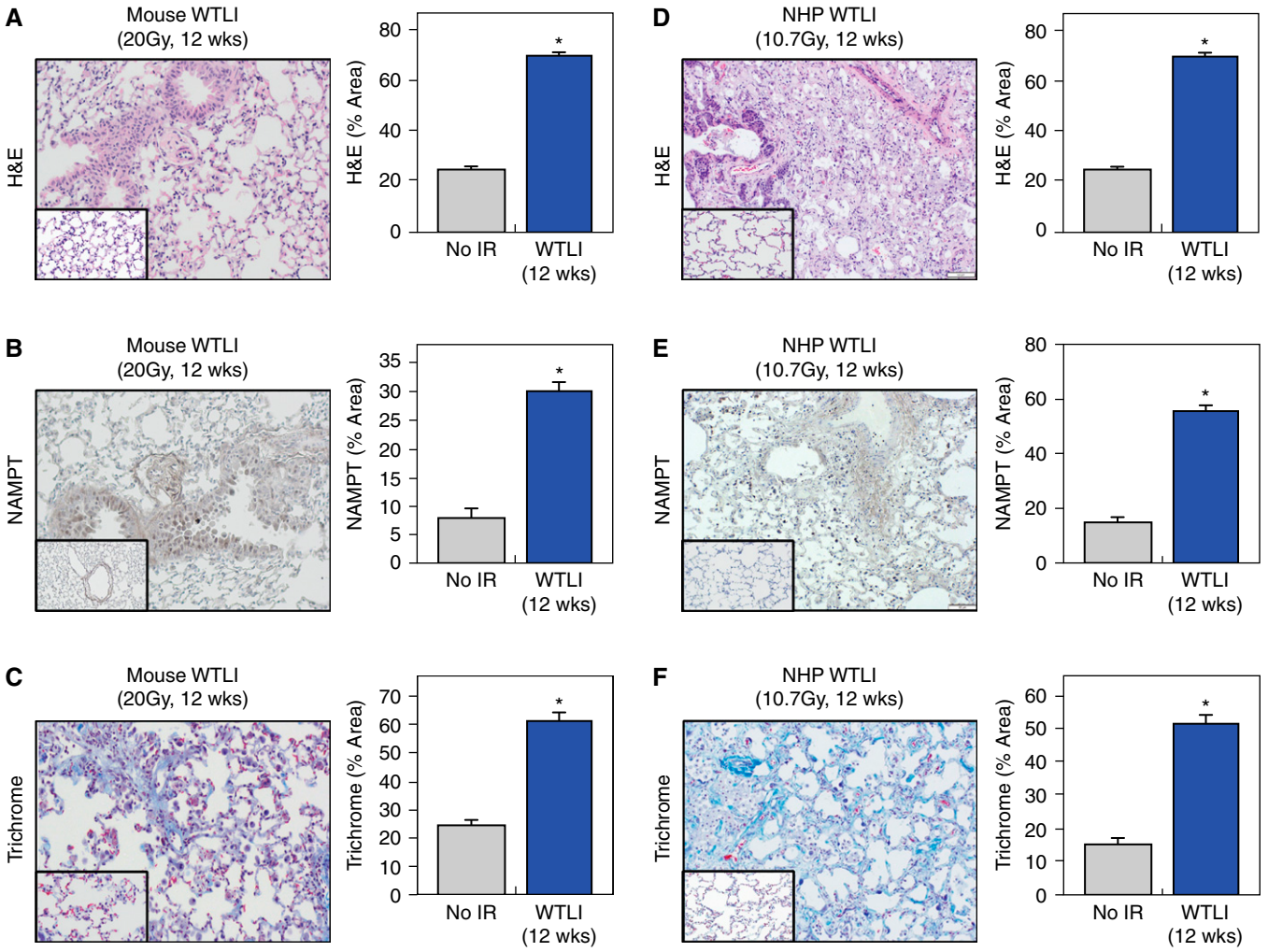

Figure 1. Thoracic irradiation exposure increases nicotinamide phosphoribosyltransferase (NAMPT) lung tissue expression and lung fibrosis in preclinical murine and nonhuman primate (NHP) models. Initial studies were designed to assess murine (C57Bl6) and *Macaca mulatta* (NHP) responses to thoracic irradiation. (*A*) Shown is representative hematoxylin and eosin (H&E) lung tissue staining (20× magnification) in an established 20-Gy whole-thorax lung irradiation (WTLI) murine model of radiation fibrosis at 12 weeks after ionizing radiation (IR) exposure (compared with sham-IR–exposed control mice, inset) showing alveolar inflammation and areas of fibrosis. ImageJ software was used to quantify the extent of hematoxylin and eosin (H&E) staining (three images from each animal, $n = 5$/group) as previously described (25). (*B*) Representative immunohistochemical (IHC) lung tissue staining of NAMPT (BLR058F, Bethyl) in C57BL/6J mice exposed to 20 Gy WTLI with ImageJ quantification. Significantly increased NAMPT expression in murine lung tissues was noted at 12 weeks after a single 20-Gy exposure (compared with control mice, inset) consistent with IR-induced NAMPT expression. (*C*) Representative trichrome blue staining image (Gomori's trichrome stain, Newcomer Supply) performed in lung tissues from 20-Gy WTLI-exposed mice with ImageJ quantification. Significantly increased trichrome blue staining was noted at 12 weeks after a single 20-Gy exposure (compared with control mice, inset). (*D*) Representative H&E lung tissue staining in NHPs (*Macaca mulatta*) 9 weeks after exposure to a single 10.7-Gy IR exposure (compared with non-IR–exposed control animals, inset). ImageJ software was used to quantify the extent of H&E staining in NHPs that exhibited alveolar inflammation, alveolar wall thickening, and areas of fibrosis. (*E*) Similar to *B*, the representative IHC NAMPT lung tissue staining image shows significantly increased NAMPT protein expression in NHPs at 10 weeks after exposure (compared with control animals, inset) with ImageJ quantification. (*F*) Similar to *C*, IHC trichrome blue staining in WTLI-exposed NHP lung tissues with ImageJ quantification showed significantly increased trichrome blue staining at 6–12 weeks after exposure (representative image shown, compared with control animals, inset) consistent with the presence of lung fibrosis. For *D–F*, three histologic or IHC images were selected for each animal and used for ImageJ quantification, with four animals/group, 8–11 weeks after WTLI. $^*P < 0.05$.

eNAMPT Neutralization Rectifies Dysregulated Lung Fibrosis–associated Protein Expression

Biochemical studies were next conducted in lung tissue homogenates to confirm eNAMPT/TLR influence on WTLI-induced fibrosis and signaling. Marked increases in smooth muscle actin (SMA) expression, a hallmark of tissue fibrosis that reflects increases in myofibroblast transition and fibrogenesis, were noted at 12 weeks after WTLI exposure in IgG control mice (Figures 3A and 3C). These changes were also accompanied by increased expression of several potent inflammatory and profibrotic mediators, such as IL-1β (Figures 3A and 3D), phosphorylated SMAD2 (Figures 3A and 3E),

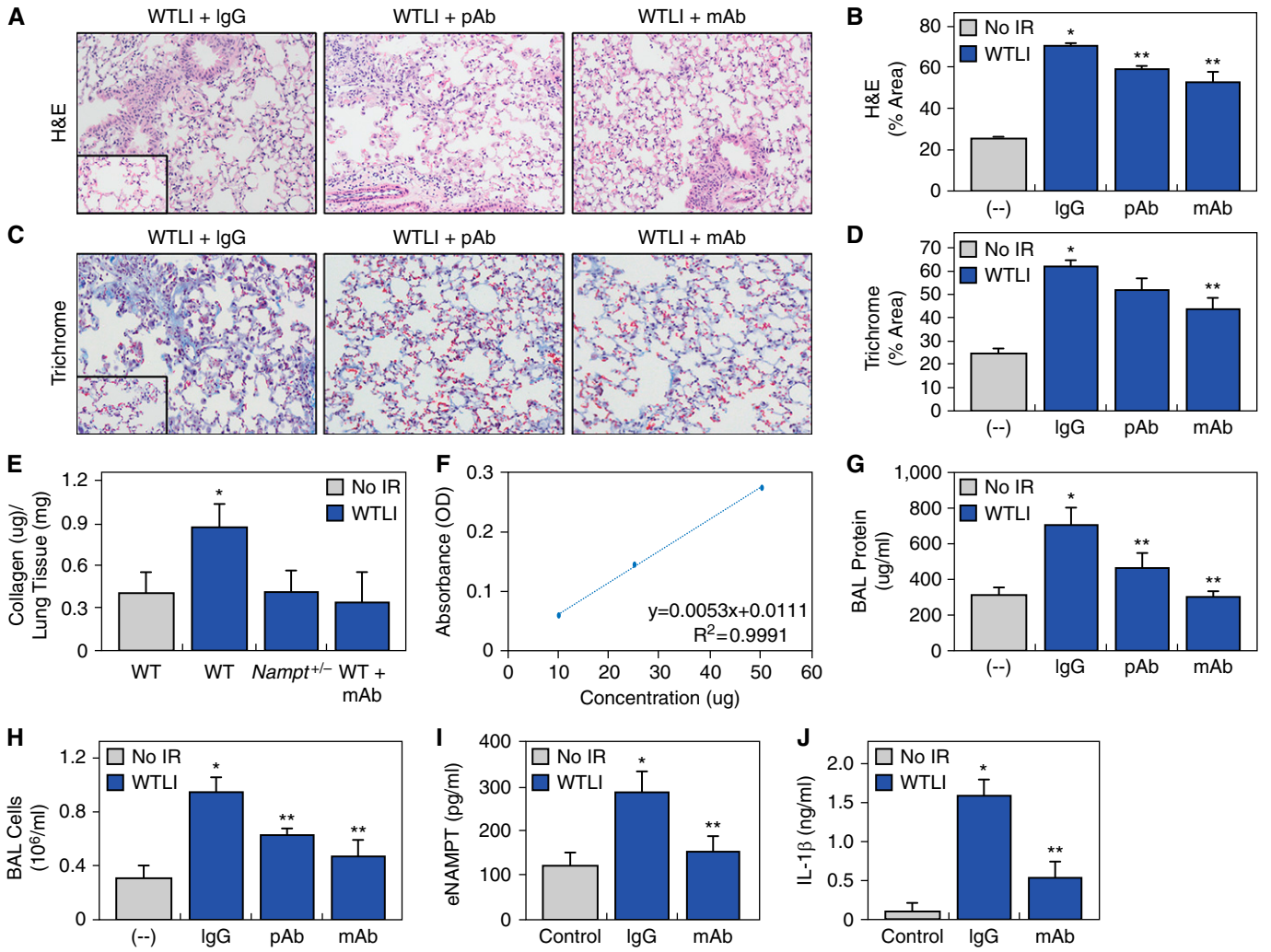

Figure 2. Extracellular NAMPT (eNAMPT) neutralization reduces the severity of preclinical WTLI-mediated murine lung fibrosis. (*A* and *B*) Similar to results described in Figure 1A, compared with sham-IR–exposed C57BL/6J mice (inset), H&E staining revealed marked increases in inflammatory lung injury and areas of fibrosis in wild-type (WT) mice exposed to 20 Gy radiation at 12 weeks (quantified by ImageJ analysis). WTLI 20 Gy–exposed WT mice receiving either the eNAMPT-neutralizing polyclonal antibody (pAb) (4 mg/kg, weekly i.p.) or the humanized monoclonal antibody (mAb) (0.4 mg/kg, weekly i.p.) demonstrated significant reductions in WTLI-mediated histologic lung injury compared with the PBS/IgG_1 control. (*C* and *D*) Similar to results described in Figure 1C, IHC studies in lung tissue from 20-Gy WTLI-exposed mice shows marked increases in trichrome blue staining with ImageJ quantification at 12 weeks (compared with control mice, inset) consistent with the presence of lung fibrosis. WTLI-exposed mice receiving the eNAMPT-neutralizing mAb (0.4 mg/kg, weekly i.p.) demonstrated significant reductions in trichrome blue staining. Mice receiving the eNAMPT pAb (4 mg/kg, weekly i.p.) showed reduced staining, which trended to significance ($P = 0.08$). (*E* and *F*) Sircol detection of murine lung tissue collagen in 12-week WTLI-exposed mice. A portion of the right lung retrieved from no-WTLI control mice and mice exposed to WTLI (20 Gy, 12 wk) was homogenized in 0.5 M acetic acid with 0.1 mg/kg of pepsin and total soluble collagen quantification performed using the Sircol kit (Biocolor Ltd.). WTLI groups included WT IgG-treated mice, *Nampt* heterozygous mice, and WT mice treated weekly with the ALT-100 mAb (0.4 mg/kg). These measurements of soluble collagen concentrations (μg), expressed per milligram lung tissue, show significantly increased soluble collagen concentrations in WT WTLI-exposed mice compared with sham-IR–exposed WT control mice (*$P < 0.05$). WTLI soluble collagen concentrations were reduced in *Nampt* heterozygous mice ($P = 0.07$) and in eNAMPT mAb-treated mice ($P = 0.09$). The standard curve for the Sircol detection of murine lung tissue collagen is displayed in *F*. (*G* and *H*) Both WTLI-mediated BAL protein concentrations and number of BAL cells were increased at 12 weeks. Mice treated with either the eNAMPT-neutralizing pAb or mAb exhibited marked reductions in BAL protein concentrations and BAL cells 12 weeks after WTLI exposure. (*I* and *J*) The Meso Scale ELISA-based Discovery platform was used to assess eNAMPT mAb effects on plasma cytokine concentrations of eNAMPT (*I*), and the inflammatory cytokine, IL-1β (*J*) in control sham-IR–exposed mice ($n = 5$), untreated 20-Gy WTLI-exposed mice receiving weekly intraperitoneal PBS/IgG_1 ($n = 7$, 12 wk), and WTLI-exposed mice receiving the eNAMPT-neutralizing mAb weekly intraperitoneally ($n = 5$, 12 wk). Exposure to 20 Gy WTLI increased plasma concentrations of eNAMPT and IL-1β, which were significantly reduced in mice receiving the eNAMPT-neutralizing mAb. *$P < 0.05$ compared with no IR and **$P < 0.05$ compared to IgG control. IgG = immunoglobulin G; OD = optical density.

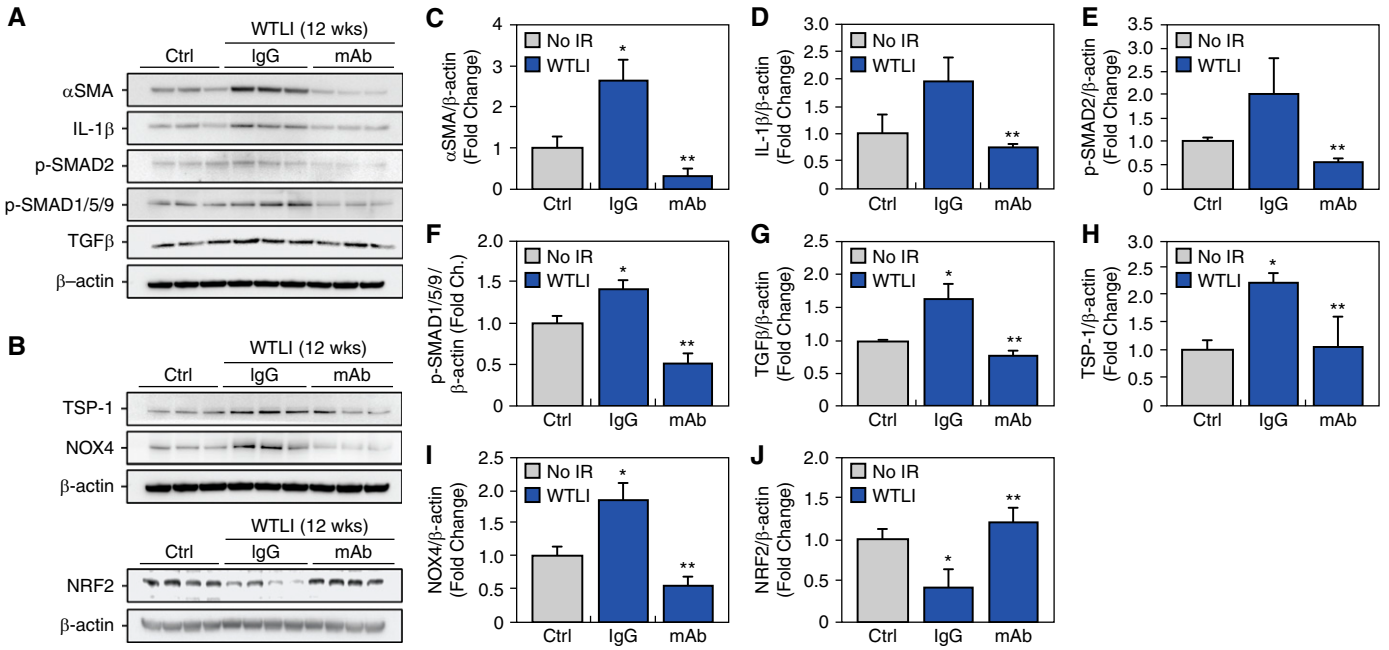

Figure 3. eNAMPT neutralization rectifies dysregulated expression of proteins involved in fibrosis/matrix-remodeling signaling pathways. Biochemical studies were next conducted in lung tissue homogenates to confirm eNAMPT/Toll-like receptor (TLR) influence on WTLI-induced dysregulated gene/protein signaling. Western blot studies of lung tissue homogenates from WTLI-exposed, PBS/IgG-, and eNAMPT mAb-treated mice ($n = 5$/group, 12 wk) were compared with sham-IR–exposed mice with representative blots ($n = 3$) shown. (*A* and *C*) Marked increases in immunoreactivity of smooth muscle actin (SMA), a hallmark of tissue fibrosis, and (*A* and *D*) the inflammatory mediator IL-1β, was noted at 12 weeks after WTLI exposure in IgG control mice. (*A* and *E*) Also noted were increased expression of TGF-β signaling pathway proteins, phosphorylated SMAD2, (*A* and *F*) phospho-SMAD1/5/9, and (*A* and *G*) TGF-β expression. WTLI-exposed mice also exhibited increased expression of the extracellular matrix protein TSP1 (thrombospondin-1) (*B* and *H*) and the reactive oxygen species (ROS)-generating NOX4 (*B* and *I*), well-known contributors to fibrosis (41–43), while demonstrating reduced expression of the ROS-sensing and transcriptional signaling molecule NRF2 (*B* and *J*). Each dysregulated protein expressed in WTLI-challenged, IgG control–treated mice was markedly rectified in mice treated weekly with the eNAMPT-neutralizing mAb (0.4 mg/kg). $^{*}P < 0.05$ compared with no IR and $^{**}P < 0.05$ compared to IgG control. Ch. = change; Ctrl = control; NOX4 = NADPH oxidase 4; TGFβ = transforming growth factor β.

phospho-SMAD1/5/9 (Figures 3A and 3F), and TGF-β (Figures 3A and 3G), findings highly consistent with activation of the fibrosis-generating TGF-β signaling pathway (13). In addition to TGF-β signaling pathway proteins, we observed WTLI-mediated increased expression of the extracellular matrix protein TSP1 (thrombospondin-1) (Figures 3B and 3H) and the ROS-generating NOX4 (Figures 3B and 3I), well-known contributors to fibrosis pathogenesis (41–43). Finally, biochemical analyses also determined WTLI exposure to reduce expression of the ROS-sensing, transcriptional signaling molecule, NRF2, in lung homogenates at 12 weeks (Figures 3B and 3J). In each case, dysregulated protein expression was restored in mice receiving the eNAMPT mAb, results highly consistent with the eNAMPT/TLR4 pathway as a trigger of WTLI-induced inflammatory cascades that contribute to the severity of WTLI-mediated RILF and confirm eNAMPT as an attractive therapeutic RILF target.

Nampt$^{+/-}$ Heterozygous Mice Are Protected from WTLI-induced Lung Fibrosis

We have previously used *Nampt*$^{+/-}$ heterozygous mice to validate NAMPT as a therapeutic target in preclinical models of ARDS (24, 26), PAH (30), and radiation pneumonitis (23). Histological lung injuries observed in WT WTLI-exposed mice at 12 weeks were significantly attenuated in WTLI-exposed *Nampt*$^{+/-}$ mice (Figures 4A and 4B), as were levels of trichrome lung tissue staining (Figures 4C and 4D), soluble lung tissue collagen (Figures 2E and 2F), BAL inflammatory indices (protein/cells) (Figures 4E and 4F) (23), and NAMPT IHC staining (Figure 4G), consistent with our prior reports (24, 25). These studies strongly support eNAMPT involvement in the development of RILF and in RILF severity.

eNAMPT/TLR4 Signaling Dysregulates Fibrosis Genes and Pathways in WTLI-induced Lung Fibrosis

We next assessed the role of circulating eNAMPT in driving gene expression that promotes the development of WTLI-induced RILF and RILF severity by examining RNAseq data from WTLI-exposed lung tissues and exploring dysregulation of lung inflammatory signaling and injury/repair processes. From a total of 561 DEGs (control vs. 12-wk WTLI; Table E1) with a false discovery rate of less than 0.05, stringency-based transcriptome filtering yielded 50 DEGs that produced the biological protein interactome network (STRING) depicted in Figure 5A. Several top prioritized DEGs are recognized as associated with fibrogenesis

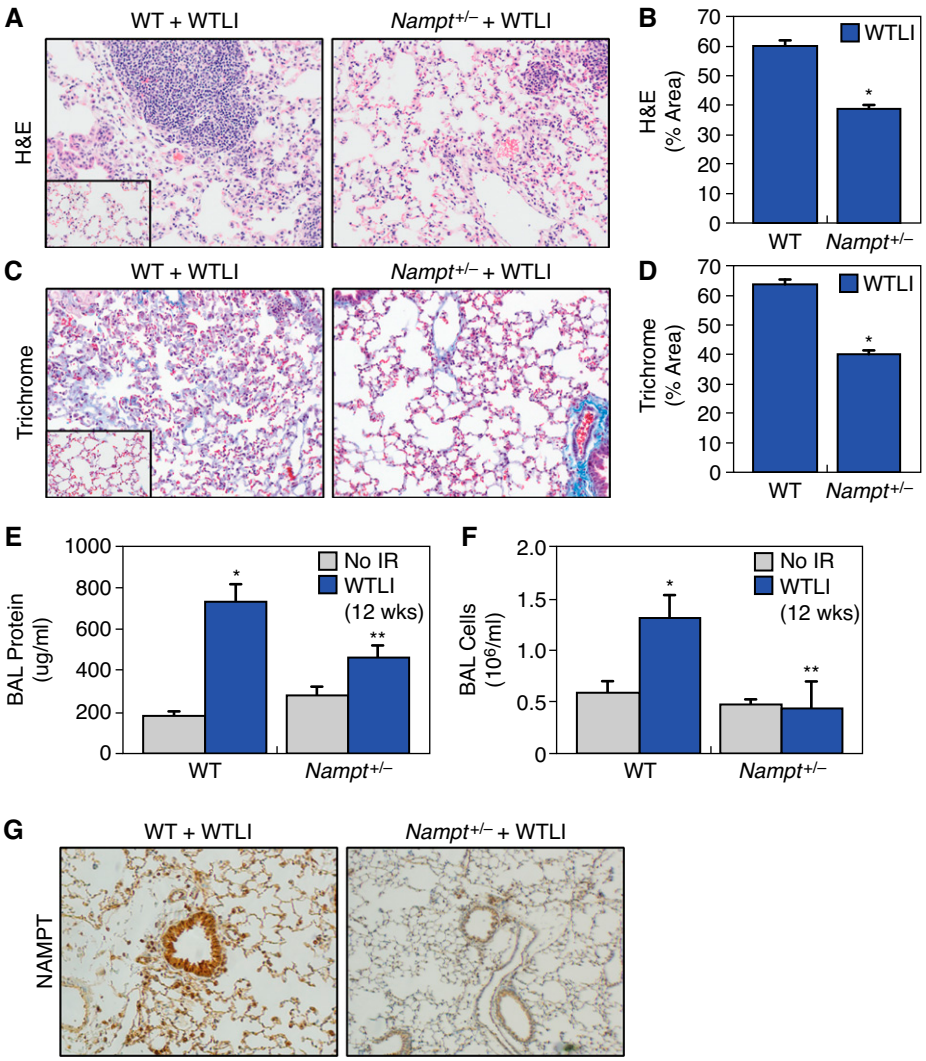

Figure 4. *Nampt*$^{+/-}$ heterozygous mice are protected from preclinical WTLI-induced lung fibrosis. As *Nampt*$^{-/-}$ homozygous knockout mice are embryonically lethal, we used *Nampt*$^{+/-}$ heterozygous mice to assess the role of NAMPT in WTLI responses as we have previously described (23, 24, 26, 30). (*A* and *B*) Histologic evidence (H&E staining) of inflammatory lung injury in WTLI (20 Gy)-exposed C57BL/6J WT mice at 12 weeks similar to that described in Figures 1A and 2A (compared with sham-IR–exposed mice, inset). WTLI-exposed *Nampt*$^{+/-}$ heterozygous mice, in contrast, exhibited significantly reduced inflammation and fibrosis compared with WT mice (ImageJ software quantification). (*C* and *D*) Similar to results described in Figures 1C and 2B, IHC studies in lung tissue from 20-Gy WTLI-exposed mice show marked increases in trichrome blue staining with ImageJ quantification at 12 weeks after 20-Gy exposure, which was significantly reduced in *Nampt*$^{+/-}$ heterozygous mice, consistent with reduced lung fibrosis. (*E* and *F*) Compared with WTLI-exposed WT mice, WTLI-exposed *Nampt*$^{+/-}$ heterozygous mice (12 wk) demonstrated significant reductions in total BAL protein/BAL cells (*$P < 0.05$ and **$P < 0.05$ compared to WT mice). (*G*) Representative IHC lung tissue staining of NAMPT exactly as described in Figure 1B. Compared with WTLI-exposed WT C57BL/6J mice, *Nampt*$^{+/-}$ heterozygous mice show significantly reduced NAMPT lung tissue expression at 12 weeks.

and fibrotic mechanisms, including the central hub gene encoding *MMP*9 (matrix metalloproteinase 9), an enzyme well known for its role in fibrogenesis (44). Additional MMP9-interacting gene/proteins known to be involved in fibrosis pathways included IL-6RA (*IL6ra*) (45), thrombospondin-1 (*Thbs1*) (46), elastin (*Eln1*) (47), and a component of the nuclear factor of activated T cells complex (*Nfatc1*) (48) (Figure 5A).

Integrating these DEG data into GO-biological–related terms demonstrated top GO terms related to the regulation of cytokine and TGF-β1 production and endothelial and smooth cell proliferation (Table 1). Pathway analysis of eNAMPT mAb-influenced WTLI-dysregulated signaling pathways (KEGG/Reactome) identified significant dysregulated pathways involved in lung fibrosis, RUNX1 (runt-related transcription factor) expression signaling, IL-1β signaling, Fra1/Fra2 transcription signaling, histone deacetylase (HDAC) signaling, immune system development, and TGF-β signaling (Figures 5B and 5C and Tables 1 and 2). Importantly, the expression of genes encoding the WTLI-induced dysregulated proteins detailed in Figure 3, as well as other fibrosis-associated proteins/genes, were

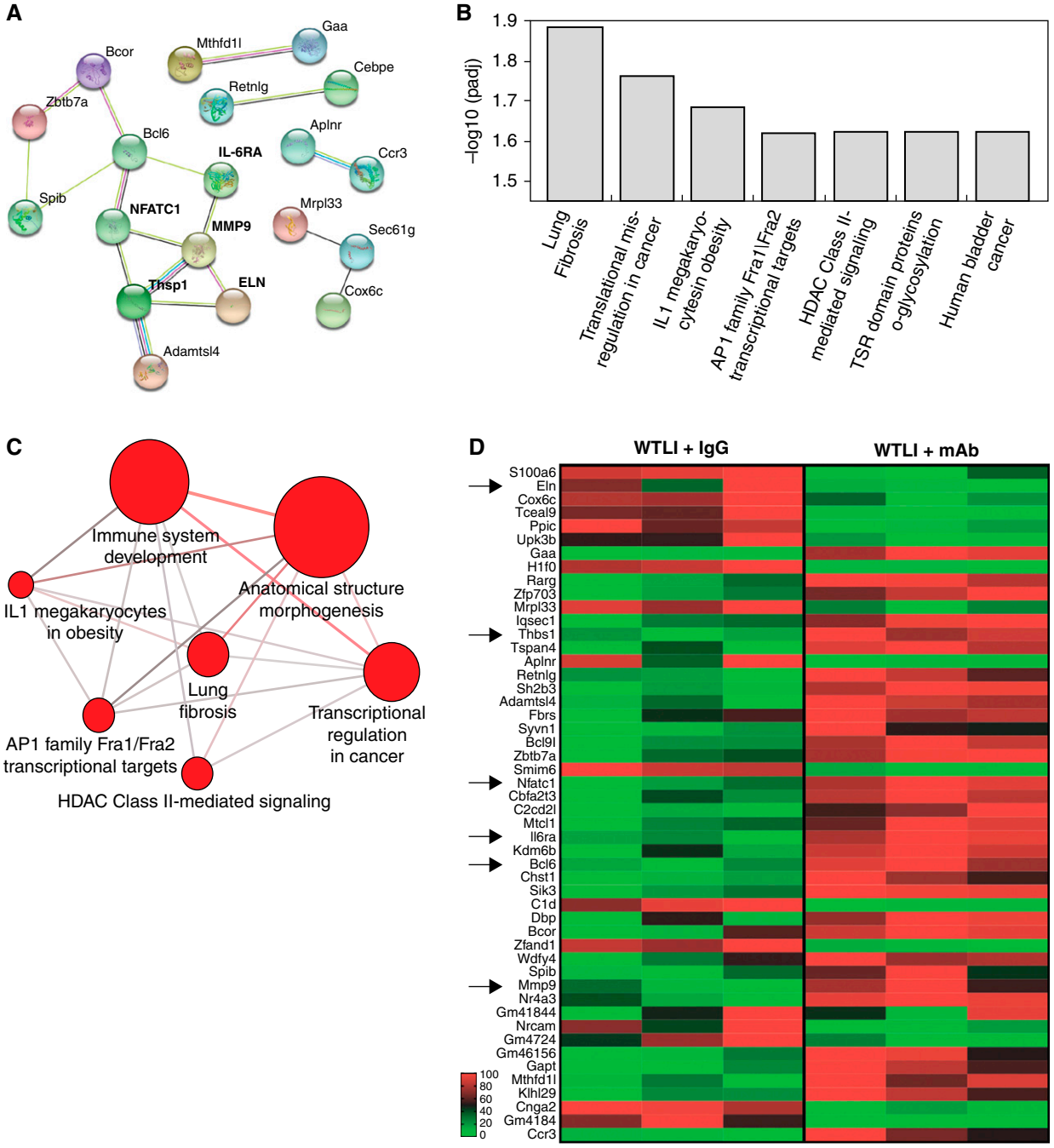

Figure 5. eNAMPT/TLR4 signaling dysregulates gene/protein signaling pathways involved in WTLI-induced lung fibrosis. RNA sequencing was used to assess eNAMPT-mediated dysregulation of lung inflammatory signaling and injury/repair processes in WTLI-exposed lung tissues from untreated mice (12 wk) and mice receiving weekly eNAMPT mAb treatment. (*A*) A total of 561 differentially expressed genes (DEGs) with a false discovery rate (FDR) less than 0.05 were identified comparing post-WTLI samples (radiated versus nonradiated) (Table E1). Further stringency-based transcriptome filtering yielded 50 DEGs comparing WTLI-exposed untreated mice to mAb-treated WTLI mice. These DEGs produced the biological protein interactome network (STRING) depicted in *A* (adjusted $P < 0.05$, fold change [FC] ± 1). Enrichment was prioritized by strength (ratio of number of proteins annotated between proteins expected annotated with this term) and FDR *P* values corrected by Benjamini-Hochberg (BH) procedure (<0.01). Network nodes represent genes, the edges indicate the functional association, and the line thickness indicates the strength of the data support. These analyses highlighted a very strong signal for matrix metalloproteinase 9 (MMP9) as a hub of eNAMPT mAb-influenced interacting genes with direct interactions with gene/proteins known to be associated with regulation of tissue fibrosis (Il6ra, Nfatc1, Eln, Thsp1). (*B* and *C*) Shown are the top Gene Ontology and Reactome pathways and biologic processes identified via analysis of the 50 DEGs. Highlighted are lung fibrosis, IL-1 signaling, Fra1/Fra2 transcription regulation, immune development, and histone deacetylase (HDAC) signaling. (*D*) Shown is the rectifying effect of the eNAMPT-neutralizing mAb on expression of 50 WTLI DEGs, which conform to pathways known to be associated with lung fibrosis, endothelial proliferation, TGF-β regulation, and angiogenesis. Arrows identify genes that are highlighted in *A* as MMP9 and MMP9-interacting proteins. Ap-1 = activator protein 1; Fra = Fos-related antigen.

Table 1. Effect of Extracellular Nicotinamide Phosphoribosyltransferase–Neutralizing Monoclonal Antibody on Whole-Thorax Lung Irradiation–induced Lung Tissue Gene Expression

Term ID	GO Biological Term	Strength	FDR	Matching Proteins
GO:0032763	Regulation of mast cell cytokine production	2.35	0.0108	Bcl6, Nr4a3
GO:1903587	Regulation of endothelial cell proliferation and angiogenesis	1.84	0.021	Thbs1, Aplnr
GO:0060351	Cartilage development involved in endochondral bone morphogenesis	1.68	0.008	Thbs1, Rarg, Sik3
GO:0030225	Macrophage differentiation	1.68	0.0308	Cebpe, Spib
GO:0030851	Granulocyte differentiation	1.68	0.0308	Cebpe, Cbfa2t3
GO:0001953	Negative regulation of cell-matrix adhesion	1.45	0.044	Bcl6, Thbs1
GO:1904707	Positive regulation of vascular smooth muscle cell proliferation	1.45	0.044	Mmp9, Nr4a3
GO:0048661	Positive regulation of smooth muscle cell proliferation	1.23	0.0108	Mmp9, Il6ra, Nr4a3, Thbs1
GO:0002573	Myeloid leukocyte differentiation	1.2	0.0126	Cbpe, Spib, Cbfa2t3, Nfatc1
GO:0017015	Regulation of TGF-β receptor signaling pathway	1.16	0.0333	Thbs1, Bcl9l, Zfp703
GO:0007369	Gastrulation	1.04	0.021	Mmp9, Nr4a3, Aplnr, Kdm6b
GO:0045766	Positive regulation of angiogenesis	1.03	0.0222	Mmp9, Ccr3, Thbs1, Aplnr
GO:0001936	Regulation of endothelial cell proliferation	1.03	0.0475	Ccr3, Thbs1, Aplnr

Definition of abbreviations: FDR = false discovery rate; GO = Gene Ontology; TGF-β = transforming growth factor-β.

markedly rectified in mice treated with the eNAMPT-neutralizing mAb (Figure 5). Figure 5D depicts a heat map of the 50 DEGs identified between WTLI-exposed IgG- and ALT-100 mAb-treated mice with the presence of several genes shown in Figure 5A with known pathway associations in lung fibrosis, endothelial-to-mesenchymal transition, TGF-β regulation, and angiogenesis. These findings are all highly consistent with activation of lung fibrosis–producing signaling pathways (13), results further supported by the increased expression of TGF-β–related genes in Table 2.

We also assessed differentially expressed miRNAs identified in blood from normal and WTLI-exposed NHPs (9.8 Gy/10.7 Gy) by limma voom analysis comparing preirradiation abundance to the indicated time point with an absolute fold change cutoff of greater than 2.25 and P value < 0.05. Six significant differentially expressed miRNAs were identified as interacting with *NAMPT* mRNA 3′UTR transcripts (40), including miR-34a-5p, miR-34c-5p, miR-139-5p, miR-199b-5p, miR-218-5p, and miR-320c (Figures E3A–E3F), with the complete list of WTLI-influenced miRNAs provided in Table E2. Each of these miRNAs exhibits known influences on fibrotic pathways, with miR34a-5p and miR-34c-5p regulating lung, renal, and liver fibrosis via modifications of the TGF-β1/Smad signaling pathway (49–51). Similarly, miR-139-5p regulates liver fibrosis via targeting the β-catenin/SOX9/TGF-β1 pathway (52, 53), and miR-199b-5p regulates left ventricular remodeling and fibrogenic responses via TGF-β–induced lung fibroblast activation (54, 55). The miR-218-5p mediates post–myocardial infarction fibrosis by targeting CX43 (56). Finally, miRNA-320a is an important regulator of the interstitial fibrotic lung disease of systemic sclerosis (57). The list of inflammatory- and fibrosis-related genes potentially influenced by each of these 6 *NAMPT*-binding miRNAs is provided in Figure 3E. Table E4 highlights the list of miRNAs that potentially influence expression of key WTLI fibrosis-related murine DEGs identified in Figure 5A. Taken together, these studies in both mice and NHPs are highly consistent with IR-induced dysregulation of key signaling pathways relevant to the development of RILF and RILF severity including *NAMPT* expression.

Discussion

Oxidative stress and immune-dysregulated inflammation are contributors to the severity of RILF (1, 15), a debilitating and potentially fatal complication of exposure to IR (2–4), as well as to the severity of idiopathic

Table 2. Effect of the Extracellular Nicotinamide Phosphoribosyltransferase–Neutralizing Monoclonal Antibody on Whole-Thorax Lung Irradiation–induced Lung Tissue Gene Expression

Pathway	*P* Value	Source	Genes	Size
RUNX1 megakaryocyte differentiation and platelet function	0.0002	Wikipathways	*NR4A3*, *THBS1*	9
Lung fibrosis	0.0005	Wikipathways	*CCR3*, *ELN*, *MMP9*, *KDM6B*	64
Transcriptional misregulation in cancer	0.0009	KEGG	*NR4A3*, *BCL6*, *CEBPE*, *MMP9*	186
IL-1 and megakaryocytes in obesity	0.0015	Wikipathways	*CCR3*, *MMP9*	24
Syndecan-4–mediated signaling events	0.0026	PID	*MMP9*, *THBS1*	32
Validated transcriptional targets of AP1 Fra1 and Fra2	0.0035	PID	*NFATC1*, *MMP9*	37
Signaling events mediated by HDAC Class II	0.0037	PID	*BCL6*, *BCOR*	38
O-glycosylation of TSR domain-containing proteins	0.0039	Reactome	*ADAMTSL4*, *THBS1*	39
Signaling by SCF-KIT	0.0047	Reactome	*SH2B3*, *MMP9*	43
Nuclear receptor transcription pathway	0.0065	Reactome	*NR4A3*, *RARG*	51
TYROBP causal network	0.0089	Wikipathways	*GAPT*, *SH2B3*	60

Definition of abbreviations: HDAC = histone deacetylase; KEGG = Kyoto Encyclopedia of Genes and Genomes; PID = Pathway Interaction Database; RUNX1 = runt-related transcription factor; SCF = stem cell factor; TSR = thrombospondin type 1 repeat.

pulmonary fibrosis (IPF) (58). In IPF, TLRs such as TLR4, which serve as pattern recognition receptors for DAMPs, are critical mediators through which DAMPs exert robust profibrotic signaling (59) and enhance TGF-β1–induced fibroblast activation. Multiple TLR4-activating DAMPs, differing in size, functionality, and primary cellular location (60), have been implicated in tissue fibrosis. Supported by studies in WTLI-exposed *Nampt*$^{+/-}$ heterozygous mice, the current study details the essential involvement of the novel DAMP and TLR4 ligand, eNAMPT (26), in the severity of WTLI-induced RILF. Robust NAMPT lung tissue expression and trichrome blue staining, reflecting collagen deposition and lung fibrosis, were observed in both WTLI-challenged mice and NHPs (Figure 1). WTLI-exposed WT C57BL6 mice receiving an eNAMPT-neutralizing antibody for 12 weeks showed significant reductions in both lung inflammatory burden (histology, BAL cells) and multiple indices of inflammation/fibrosis including trichrome staining, soluble collagen, SMA and TGF-β lung tissue concentrations, and circulating concentrations of eNAMPT and IL-1β. The eNAMPT mAb also reduced expression of the ROS-generating NOX4, while preserving lung concentrations of the antioxidant transcription factor NRF2, compatible with eNAMPT mAb-mediated attenuation of ROS-induced fibrosis-promoting pathways (61, 62).

WTLI-mediated NAMPT lung tissue expression rapidly peaks at 2 weeks (23); however, the mechanisms underlying the persistent radiation-induced NAMPT protein expression in both mice and NHPs (over 12 wk) are unknown but may reflect epigenetic *NAMPT* regulation as suggested by our miRNA profiling studies in WTLI-exposed NHPs (Table E2), which identified several differentially expressed miRNAs, proven to interact with the *NAMPT* 3′UTR and each linked to inflammation and tissue remodeling with significant influences on TGF-β1 signaling and tissue fibrosis (Figure E3) (50, 63). Interestingly, our previous profiling of WTLI-induced miRNAs (64), included prominent representation of miRNAs that regulate fibrosis and inflammation. One of those miRNAs that contributed most strongly to the survival prediction was miR-34a-5p, a *NAMPT* 3′UTR binding miRNA (Figure E3) that influences a number of fibrosis-related genes in our RNAseq dataset (Table E4). Beyond miRNA regulation of *NAMPT* expression, we have previously shown that transcription factors associated with radiation responses (65), such as STAT family, SOX family, NRF2, NF-κB, and HIF-2α, each regulate *NAMPT* transcription (31, 66, 67).

Our genome-wide expression studies and biochemical analyses of murine lung tissues (at 12 wk) corroborate earlier reports (13) demonstrating dysregulated oxidant stress and immune system processes and highlight profibrotic TGF-β signaling involvement in RILF severity, consistent with multiple models of lung fibrosis. TGF-β drives epithelial–mesenchymal transition, differentiation of fibroblasts into α-SMA–expressing myofibroblasts (68), and secretion of excess collagen, fibronectin, and proteoglycans, which increases lung tissue stiffness. Studies using the fibrosis-reducing eNAMPT-neutralizing mAb showed attenuation of IR-induced TGF-β signaling gene expression (*Thbs1*, *Bcl9l*, *Zfp703*; Table 2) and protein expression of TGF-β, p-Smad2, and p-Smad1/5/9 (Figure 5).

In addition to the TGF-β signaling pathway, other proinflammatory cytokines, such as the IL-1β signaling pathway, are regulated by oxidative stress and redox signaling and contribute to tissue fibrosis via T cell and fibroblast activation and release of profibrotic cytokines including TGF-β1 (69). The IL-1β signaling pathway was highlighted by genomic and biochemical studies showing increased gene expression (Figures 5B and 5C) and protein concentrations of IL-1β observed in WTLI lung homogenates (Figure 3A), with these findings all nearly normalized in mice receiving the eNAMPT-neutralizing mAb. These RILF findings are in strong synchrony with genomic and biochemical analyses of murine radiation pneumonitis (23), with elevated plasma IL-1β concentrations and *IL1β* identified as a central prioritized DEG, findings once again reduced in WTLI mice treated with the eNAMPT mAb. Together, these analyses highlight a very strong signal for IL-1β as a key eNAMPT mAb-influenced interacting gene/protein involved in both radiation pneumonitis and RILF.

Inhibition of matrix synthesis and reduced inflammation are primary therapeutic goals to decrease RILF severity. TGF-β signaling promotes the decreased activity of matrix-degrading enzymes, such as MMP-2 and MMP-9, and increased activity of tissue inhibitors of metalloproteinases (TIMPs), compounding the ongoing excessive matrix deposition (70). *MMP9* was a central STRING interactome hub gene in the RILF murine model (Figure 5A) and *MMP12* a top WTLI-mediated dysregulated gene in murine radiation pneumonitis (23). It is interesting to note that each STRING interactome gene/protein directly interacting with MMP9 has been strongly implicated in influencing lung fibrotic pathways. For example, elastin (*ELN*) is the main constituent of elastic connective tissue relevant to organ fibrosis (47). The IL-6 receptor α subunit (*Il6ra*) contributes to inflammatory signaling promoting pulmonary fibrosis (71) and influences IPF mortality (72). Thrombospondin 1 (*Thbs1*), a previously identified dysregulated RILF gene (19), is a matrix protein that mediates cell-to-cell and cell-to-matrix interactions binding to fibrinogen, fibronectin, laminin, and multiple collagen types and integrins and regulates tissue fibrosis and latent TGF-β activation. NFATC1 (*NFATC1*) is a component of the nuclear factor of activated T cells DNA-binding transcription cytosolic complex, a major immunosuppression molecular target, that induces gene transcription during immune responses in the early stages of IPF (73, 74).

Other genes that were identified in the STRING interactome and pathway analysis but that do not directly connect to *MMP9* are also linked to fibrosis. For example, *Ccr3* is a chemokine receptor that binds eotaxin (CCL11), a therapeutic target in IPF (75), and *Aplnr* (76) encodes APJ, a receptor for apelin, a signaling pathway that counteracts TGF-β signaling and tissue fibrosis. *Cox6c* is a cytochrome oxidase involved in tissue fibrosis development (77), and *Spib* and *Zbtb7a* (78) are transcription factors that drive profibrotic gene expression, including expression of *MUC5B*, a gene/protein we have shown related to IPF severity (79, 80). Finally, WTLI dysregulated processes included Fra1/Fra, two transcription factors that are AP-1 family members encoded by *FOSL1* (Fos-related antigen) and enhance transcription of cytokine and chemokine genes involved in inflammation, extracellular remodeling, early profibrotic collagen transcription (81), and the severity of pulmonary fibrosis (82). Thus, genomic and biochemical studies highlight genes/proteins and fibrotic signaling pathways that are differentially influenced by inhibition of eNAMPT/TLR4 signaling, consistent with

eNAMPT/TLR4 signaling contributing to the severity of RILF (59, 83, 84).

Our study exhibits several limitations, including the absence of defining the WTLI-responsive target cells involved in eNAMPT secretion and the exact TLR4 receptor-expressing cells involved in eNAMPT-driven RILF responses. Our prior studies in models of inflammatory lung injury have highlighted NAMPT expression primarily in lung epithelium, lung endothelium, and inflammatory leukocytes, findings consistent with the IHC results described in Figure 1. We have previously used an endothelial-specific knockout mouse to demonstrate the prominent contribution of endothelial cell secretion of eNAMPT into the circulation to produce inflammatory lung injury (25). Given the ubiquity of TLR4 receptor expression, it is difficult to define the main TLR4-expressing target cells for eNAMPT ligation. However, in addition to epithelium, endothelium, and inflammatory leukocytes, lung fibroblasts are additional key potential targets, as we have shown eNAMPT to induce endothelial-to-mesenchymal transition and myofibroblast conversion (31).

An additional limitation of our genomic work is the potential confounding effect of fibrosis-inducing changes in the cellular composition of lung tissues used for bulk RNAseq. As opposed to single-cell transcriptomics, this approach limits the defining of the exact cells contributing to WTLI-induced DEGs. The value of this bulk RNAseq approach, however, is the capacity to capture the most highly DEGs regardless of the cells of origin, which in our studies served to corroborate the importance of eNAMPT/TLR4 signaling in regulating key fibrosis genes and proteins.

In summary, using a well-established and informative murine WTLI model of RILF (8, 16–20, 85), our studies provide strong support for secreted eNAMPT, a novel DAMP and ligand for the pattern-recognition receptor TLR4, as a highly druggable therapeutic target in RILF. We speculate that eNAMPT-triggered inflammation dysregulates signaling pathway genes and proteins that initiate fibrogenesis and disrupts fibrosis/remodeling resolution resulting in self-perpetuating cycles of inflammation, connective tissue deposition, and fibrosis. Our data confirm a humanized eNAMPT-neutralizing mAb as a therapeutic strategy to significantly reduce the severity of RILF by suppressing TGF-β–, IL-1β–, and ROS-mediated fibrogenic signaling pathways. We have previously identified plasma eNAMPT concentrations as a potentially valuable biomarker of radiation pneumonitis risk/severity (23) and specific *NAMPT* SNPs as a high-risk genotype for ARDS and PAH mortality (29, 31, 67). Thus, the tools exist for precision medicine approaches to identify individuals undergoing radiotherapy at high risk for developing RILF as likely responders to eNAMPT-neutralizing mAb therapy, a personalized path to address this serious unmet medical and societal need. ■

Author disclosures are available with the text of this article at www.atsjournals.org.

References

1. Cytlak UM, Dyer DP, Honeychurch J, Williams KJ, Travis MA, Illidge TM. Immunomodulation by radiotherapy in tumour control and normal tissue toxicity. *Nat Rev Immunol* [online ahead of print] 1 Jul 2021; DOI: 10.1038/s41577-021-00568-1.
2. Giuranno L, Ient J, De Ruysscher D, Vooijs MA. Radiation-induced lung injury (RILI). *Front Oncol* 2019;9:877.
3. Hanania AN, Mainwaring W, Ghebre YT, Hanania NA, Ludwig M. Radiation-induced lung injury: assessment and management. *Chest* 2019;156:150–162.
4. Keffer S, Guy CL, Weiss E. Fatal radiation pneumonitis: literature review and case series. *Adv Radiat Oncol* 2019;5:238–249.
5. Rodrigues G, Lock M, D'Souza D, Yu E, Van Dyk J. Prediction of radiation pneumonitis by dose - volume histogram parameters in lung cancer: a systematic review. *Radiother Oncol* 2004;71:127–138.
6. Gao F, Fish BL, Moulder JE, Jacobs ER, Medhora M. Enalapril mitigates radiation-induced pneumonitis and pulmonary fibrosis if started 35 days after whole-thorax irradiation. *Radiat Res* 2013;180:546–552.
7. Li M, Abdollahi A, Gröne HJ, Lipson KE, Belka C, Huber PE. Late treatment with imatinib mesylate ameliorates radiation-induced lung fibrosis in a mouse model. *Radiat Oncol* 2009;4:66.
8. Mathew B, Huang Y, Jacobson JR, Berdyshev E, Gerhold LM, Wang T, *et al.* Simvastatin attenuates radiation-induced murine lung injury and dysregulated lung gene expression. *Am J Respir Cell Mol Biol* 2011;44:415–422.
9. Okunieff P, Augustine E, Hicks JE, Cornelison TL, Altemus RM, Naydich BG, *et al.* Pentoxifylline in the treatment of radiation-induced fibrosis. *J Clin Oncol* 2004;22:2207–2213.
10. Zeng W, Liu Z, Dai H, Yan M, Luo H, Ke M, *et al.* Anti-fibrotic, anti-VEGF or radiotherapy treatments as adjuvants for pterygium excision: a systematic review and network meta-analysis. *BMC Ophthalmol* 2017;17:211.
11. Mahmood J, Jelveh S, Calveley V, Zaidi A, Doctrow SR, Hill RP. Mitigation of lung injury after accidental exposure to radiation. *Radiat Res* 2011;176:770–780.
12. Huang Y, Zhang W, Yu F, Gao F. The cellular and molecular mechanism of radiation-induced lung injury. *Med Sci Monit* 2017;23:3446–3450.
13. Straub JM, New J, Hamilton CD, Lominska C, Shnayder Y, Thomas SM. Radiation-induced fibrosis: mechanisms and implications for therapy. *J Cancer Res Clin Oncol* 2015;141:1985–1994.
14. Bime C, Casanova NG, Nikolich-Zugich J, Knox KS, Camp SM, Garcia JGN. Strategies to DAMPen COVID-19-mediated lung and systemic inflammation and vascular injury. *Transl Res* 2021;232:37–48.
15. Lierova A, Jelicova M, Nemcova M, Proksova M, Pejchal J, Zarybnicka L, *et al.* Cytokines and radiation-induced pulmonary injuries. *J Radiat Res (Tokyo)* 2018;59:709–753.
16. Wang T, Mathew B, Wu X, Shimizu Y, Rizzo AN, Dudek SM, *et al.* Nonmuscle myosin light chain kinase activity modulates radiation-induced lung injury. *Pulm Circ* 2016;6:234–239.
17. Mathew B, Jacobson JR, Siegler JH, Moitra J, Blasco M, Xie L, *et al.* Role of migratory inhibition factor in age-related susceptibility to radiation lung injury via NF-E2-related factor-2 and antioxidant regulation. *Am J Respir Cell Mol Biol* 2013;49:269–278.
18. Mathew B, Takekoshi D, Sammani S, Epshtein Y, Sharma R, Smith BD, *et al.* Role of GADD45a in murine models of radiation- and bleomycin-induced lung injury. *Am J Physiol Lung Cell Mol Physiol* 2015;309:L1420–L1429.
19. Gorshkova I, Zhou T, Mathew B, Jacobson JR, Takekoshi D, Bhattacharya P, *et al.* Inhibition of serine palmitoyltransferase delays the onset of radiation-induced pulmonary fibrosis through the negative regulation of sphingosine kinase-1 expression. *J Lipid Res* 2012;53:1553–1568.
20. Mathew B, Jacobson JR, Berdyshev E, Huang Y, Sun X, Zhao Y, *et al.* Role of sphingolipids in murine radiation-induced lung injury: protection by sphingosine 1-phosphate analogs. *FASEB J* 2011;25:3388–3400.
21. Bolourani S, Brenner M, Wang P. The interplay of DAMPs, TLR4, and proinflammatory cytokines in pulmonary fibrosis. *J Mol Med (Berl)* 2021;99:1373–1384.
22. Ellson CD, Dunmore R, Hogaboam CM, Sleeman MA, Murray LA. Danger-associated molecular patterns and danger signals in idiopathic pulmonary fibrosis. *Am J Respir Cell Mol Biol* 2014;51:163–168.

23. Garcia AN, Casanova NG, Valera DG, Sun X, Song JH, Kempf CL, *et al.* Involvement of eNAMPT/TLR4 signaling in murine radiation pneumonitis: protection by eNAMPT neutralization. *Transl Res* 2022; 239:44–57.
24. Hong SB, Huang Y, Moreno-Vinasco L, Sammani S, Moitra J, Barnard JW, *et al.* Essential role of pre-B-cell colony enhancing factor in ventilator-induced lung injury. *Am J Respir Crit Care Med* 2008;178: 605–617.
25. Quijada H, Bermudez T, Kempf CL, Valera DG, Garcia AN, Camp SM, *et al.* Endothelial eNAMPT amplifies pre-clinical acute lung injury: efficacy of an eNAMPT-neutralising monoclonal antibody. *Eur Respir J* 2021;57:2002536.
26. Camp SM, Ceco E, Evenoski CL, Danilov SM, Zhou T, Chiang ET, *et al.* Unique Toll-like receptor 4 activation by NAMPT/PBEF induces NFκB signaling and inflammatory lung injury. *Sci Rep* 2015;5:13135.
27. Bajwa EK, Yu CL, Gong MN, Thompson BT, Christiani DC. Pre-B-cell colony-enhancing factor gene polymorphisms and risk of acute respiratory distress syndrome. *Crit Care Med* 2007;35:1290–1295.
28. Bime C, Casanova N, Oita RC, Ndukum J, Lynn H, Camp SM, *et al.* Development of a biomarker mortality risk model in acute respiratory distress syndrome. *Crit Care* 2019;23:410.
29. Ye SQ, Simon BA, Maloney JP, Zambelli-Weiner A, Gao L, Grant A, *et al.* Pre-B-cell colony-enhancing factor as a potential novel biomarker in acute lung injury. *Am J Respir Crit Care Med* 2005;171:361–370.
30. Chen J, Sysol JR, Singla S, Zhao S, Yamamura A, Valdez-Jasso D, *et al.* Nicotinamide phosphoribosyltransferase promotes pulmonary vascular remodeling and is a therapeutic target in pulmonary arterial hypertension. *Circulation* 2017;135:1532–1546.
31. Sun X, Sun BL, Babicheva A, Vanderpool R, Oita RC, Casanova N, *et al.* Direct extracellular NAMPT involvement in pulmonary hypertension and vascular remodeling: transcriptional regulation by SOX and HIF-2α. *Am J Respir Cell Mol Biol* 2020;63:92–103.
32. Sun BL, Sun X, Casanova N, Garcia AN, Oita R, Algotar AM, *et al.* Role of secreted extracellular nicotinamide phosphoribosyltransferase (eNAMPT) in prostate cancer progression: novel biomarker and therapeutic target. *EBioMedicine* 2020;61:103059.
33. Colombo G, Clemente N, Zito A, Bracci C, Colombo FS, Sangaletti S, *et al.* Neutralization of extracellular NAMPT (nicotinamide phosphoribosyltransferase) ameliorates experimental murine colitis. *J Mol Med (Berl)* 2020;98:595–612.
34. de Faria EB, Barrow KR, Ruehle BT, Parker JT, Swartz E, Taylor-Howell C, *et al.* The evolving Mcart multimodal imaging core: establishing a protocol for computed tomography and echocardiography in the rhesus macaque to perform longitudinal analysis of radiation-induced organ injury. *Health Phys* 2015;109:479–492.
35. Garofalo M, Bennett A, Farese AM, Harper J, Ward A, Taylor-Howell C, *et al.* The delayed pulmonary syndrome following acute high-dose irradiation: a rhesus macaque model. *Health Phys* 2014;106:56–72.
36. Rehan M, Kurundkar D, Kurundkar AR, Logsdon NJ, Smith SR, Chanda D, *et al.* Restoration of SIRT3 gene expression by airway delivery resolves age-associated persistent lung fibrosis in mice. *Nat Aging* 2021;1:205–217.
37. Du J, Yuan Z, Ma Z, Song J, Xie X, Chen Y. KEGG-PATH: Kyoto encyclopedia of genes and genomes-based pathway analysis using a path analysis model. *Mol Biosyst* 2014;10:2441–2447.
38. Fabregat A, Sidiropoulos K, Viteri G, Forner O, Marin-Garcia P, Arnau V, *et al.* Reactome pathway analysis: a high-performance in-memory approach. *BMC Bioinformatics* 2017;18:142.
39. Szklarczyk D, Morris JH, Cook H, Kuhn M, Wyder S, Simonovic M, *et al.* The STRING database in 2017: quality-controlled protein-protein association networks, made broadly accessible. *Nucleic Acids Res* 2017;45:D362–D368.
40. Adyshev DM, Elangovan VR, Moldobaeva N, Mapes B, Sun X, Garcia JG. Mechanical stress induces pre-B-cell colony-enhancing factor/NAMPT expression via epigenetic regulation by miR-374a and miR-568 in human lung endothelium. *Am J Respir Cell Mol Biol* 2014;50:409–418.
41. Kolb M, Margetts PJ, Anthony DC, Pitossi F, Gauldie J. Transient expression of IL-1beta induces acute lung injury and chronic repair leading to pulmonary fibrosis. *J Clin Invest* 2001;107:1529–1536.
42. Liu W, Ding I, Chen K, Olschowka J, Xu J, Hu D, *et al.* Interleukin 1beta (IL1B) signaling is a critical component of radiation-induced skin fibrosis. *Radiat Res* 2006;165:181–191.
43. Murphy-Ullrich JE, Suto MJ. Thrombospondin-1 regulation of latent TGF-β activation: a therapeutic target for fibrotic disease. *Matrix Biol* 2018; 68-69:28–43.
44. Yue H, Hu K, Liu W, Jiang J, Chen Y, Wang R. Role of matrix metalloproteinases in radiation-induced lung injury in alveolar epithelial cells of Bama minipigs. *Exp Ther Med* 2015;10:1437–1444.
45. Le TT, Karmouty-Quintana H, Melicoff E, Le TT, Weng T, Chen NY, *et al.* Blockade of IL-6 trans signaling attenuates pulmonary fibrosis. *J Immunol* 2014;193:3755–3768.
46. Murphy-Ullrich JE. Thrombospondin 1 and its diverse roles as a regulator of extracellular matrix in fibrotic disease. *J Histochem Cytochem* 2019; 67:683–699.
47. Chen W, Yan X, Xu A, Sun Y, Wang B, Huang T, *et al.* Dynamics of elastin in liver fibrosis: accumulates late during progression and degrades slowly in regression. *J Cell Physiol* 2019;234:22613–22622.
48. Fujimoto H, D'Alessandro-Gabazza CN, Palanki MS, Erdman PE, Takagi T, Gabazza EC, *et al.* Inhibition of nuclear factor-kappaB in T cells suppresses lung fibrosis. *Am J Respir Crit Care Med* 2007;176: 1251–1260.
49. Feili X, Wu S, Ye W, Tu J, Lou L. MicroRNA-34a-5p inhibits liver fibrosis by regulating TGF-β1/Smad3 pathway in hepatic stellate cells. *Cell Biol Int* 2018;42:1370–1376.
50. Hu RP, Lu YY, Zhang XJ. MiR-34b-5p knockdown attenuates bleomycin-induced pulmonary fibrosis by targeting tissue inhibitor of metalloproteinase 3 (TIMP3). *Eur Rev Med Pharmacol Sci* 2019;23: 2273–2279.
51. Park EJ, Jung HJ, Choi HJ, Cho JI, Park HJ, Kwon TH. miR-34c-5p and CaMKII are involved in aldosterone-induced fibrosis in kidney collecting duct cells. *Am J Physiol Renal Physiol* 2018;314:F329–F342.
52. He C, Shu B, Zhou Y, Zhang R, Yang X. The miR-139-5p/peripheral myelin protein 22 axis modulates TGF-β-induced hepatic stellate cell activation and CCl_4-induced hepatic fibrosis in mice. *Life Sci* 2021;276: 119294.
53. Wang Q, Wei S, Li L, Bu Q, Zhou H, Su W, *et al.* miR-139-5p sponged by LncRNA NEAT1 regulates liver fibrosis via targeting β-catenin/SOX9/ TGF-β1 pathway. *Cell Death Discov* 2021;7:243.
54. Duygu B, Poels EM, Juni R, Bitsch N, Ottaviani L, Olieslagers S, *et al.* miR-199b-5p is a regulator of left ventricular remodeling following myocardial infarction. *Noncoding RNA Res* 2017;2:18–26.
55. Lino Cardenas CL, Henaoui IS, Courcot E, Roderburg C, Cauffiez C, Aubert S, *et al.* miR-199a-5p Is upregulated during fibrogenic response to tissue injury and mediates TGFbeta-induced lung fibroblast activation by targeting caveolin-1. *PLoS Genet* 2013;9:e1003291.
56. Sun B, Zhao C, Mao Y. miR-218-5p mediates myocardial fibrosis after myocardial infarction by targeting CX43. *Curr Pharm Des* 2021;27: 4504–4512.
57. Li Y, Huang J, Hu C, Zhou J, Xu D, Hou Y, *et al.* MicroRNA-320a: an important regulator in the fibrotic process in interstitial lung disease of systemic sclerosis. *Arthritis Res Ther* 2021;23:21.
58. Noth I, Zhang Y, Ma SF, Flores C, Barber M, Huang Y, *et al.* Genetic variants associated with idiopathic pulmonary fibrosis susceptibility and mortality: a genome-wide association study. *Lancet Respir Med* 2013; 1:309–317.
59. Bhattacharyya S, Wang W, Qin W, Cheng K, Coulup S, Chavez S, *et al.* TLR4-dependent fibroblast activation drives persistent organ fibrosis in skin and lung. *JCI Insight* 2018;3:e98850.
60. Hamada N, Maeyama T, Kawaguchi T, Yoshimi M, Fukumoto J, Yamada M, *et al.* The role of high mobility group box1 in pulmonary fibrosis. *Am J Respir Cell Mol Biol* 2008;39:440–447.
61. Gonzalez-Gonzalez FJ, Chandel NS, Jain M, Budinger GRS. Reactive oxygen species as signaling molecules in the development of lung fibrosis. *Transl Res* 2017;190:61–68.
62. Jarman ER, Khambata VS, Cope C, Jones P, Roger J, Ye LY, *et al.* An inhibitor of NADPH oxidase-4 attenuates established pulmonary fibrosis in a rodent disease model. *Am J Respir Cell Mol Biol* 2014;50:158–169.
63. Bian H, Zhou Y, Zhou D, Zhang Y, Shang D, Qi J. The latest progress on miR-374 and its functional implications in physiological and pathological processes. *J Cell Mol Med* 2019;23:3063–3076.
64. Rogers CJ, Lukaszewicz AI, Yamada-Hanff J, Micewicz ED, Ratikan JA, Starbird MA, *et al.* Identification of miRNA signatures associated with radiation-induced late lung injury in mice. *PLoS One* 2020;15: e0232411.

65. Hellweg CE, Spitta LF, Henschenmacher B, Diegeler S, Baumstark-Khan C. Transcription factors in the cellular response to charged particle exposure. *Front Oncol* 2016;6:61.
66. Elangovan VR, Camp SM, Kelly GT, Desai AA, Adyshev D, Sun X, *et al.* Endotoxin- and mechanical stress-induced epigenetic changes in the regulation of the nicotinamide phosphoribosyltransferase promoter. *Pulm Circ* 2016;6:539–544.
67. Sun X, Elangovan VR, Mapes B, Camp SM, Sammani S, Saadat L, *et al.* The NAMPT promoter is regulated by mechanical stress, signal transducer and activator of transcription 5, and acute respiratory distress syndrome-associated genetic variants. *Am J Respir Cell Mol Biol* 2014;51:660–667.
68. Rifkin DB, Rifkin WJ, Zilberberg L. LTBPs in biology and medicine: LTBP diseases. *Matrix Biol* 2018;71-72:90–99.
69. Murthy S, Adamcakova-Dodd A, Perry SS, Tephly LA, Keller RM, Metwali N, *et al.* Modulation of reactive oxygen species by Rac1 or catalase prevents asbestos-induced pulmonary fibrosis. *Am J Physiol Lung Cell Mol Physiol* 2009;297:L846–L855.
70. Pardo A, Selman M. Matrix metalloproteases in aberrant fibrotic tissue remodeling. *Proc Am Thorac Soc* 2006;3:383–388.
71. Pedroza M, Schneider DJ, Karmouty-Quintana H, Coote J, Shaw S, Corrigan R, *et al.* Interleukin-6 contributes to inflammation and remodeling in a model of adenosine mediated lung injury. *PLoS One* 2011;6:e22667.
72. Papiris SA, Tomos IP, Karakatsani A, Spathis A, Korbila I, Analitis A, *et al.* High levels of IL-6 and IL-8 characterize early-on idiopathic pulmonary fibrosis acute exacerbations. *Cytokine* 2018;102: 168–172.
73. Hogan PG. Calcium-NFAT transcriptional signalling in T cell activation and T cell exhaustion. *Cell Calcium* 2017;63:66–69.
74. Szema AM, Forsyth E, Ying B, Hamidi SA, Chen JJ, Hwang S, *et al.* NFATc3 and VIP in idiopathic pulmonary fibrosis and chronic obstructive pulmonary disease. *PLoS One* 2017;12:e0170606.
75. Huaux F, Gharaee-Kermani M, Liu T, Morel V, McGarry B, Ullenbruch M, *et al.* Role of eotaxin-1 (CCL11) and CC chemokine receptor 3 (CCR3) in bleomycin-induced lung injury and fibrosis. *Am J Pathol* 2005;167: 1485–1496.
76. Yokoyama Y, Sekiguchi A, Fujiwara C, Uchiyama A, Uehara A, Ogino S, *et al.* Inhibitory regulation of skin fibrosis in systemic sclerosis by apelin/APJ signaling. *Arthritis Rheumatol* 2018;70:1661–1672.
77. Tian BX, Sun W, Wang SH, Liu PJ, Wang YC. Differential expression and clinical significance of COX6C in human diseases. *Am J Transl Res* 2021;13:1–10.
78. Zhang Y, Noth I, Garcia JG, Kaminski N. A variant in the promoter of MUC5B and idiopathic pulmonary fibrosis. *N Engl J Med* 2011;364: 1576–1577.
79. Helling BA, Gerber AN, Kadiyala V, Sasse SK, Pedersen BS, Sparks L, *et al.* Regulation of MUC5B expression in idiopathic pulmonary fibrosis. *Am J Respir Cell Mol Biol* 2017;57:91–99.
80. McDonough JE, Kaminski N, Thienpont B, Hogg JC, Vanaudenaerde BM, Wuyts WA. Gene correlation network analysis to identify regulatory factors in idiopathic pulmonary fibrosis. *Thorax* 2019;74: 132–140.
81. Ucero AC, Bakiri L, Roediger B, Suzuki M, Jimenez M, Mandal P, *et al.* Fra-2-expressing macrophages promote lung fibrosis in mice. *J Clin Invest* 2019;129:3293–3309.
82. Rajasekaran S, Reddy NM, Zhang W, Reddy SP. Expression profiling of genes regulated by Fra-1/AP-1 transcription factor during bleomycin-induced pulmonary fibrosis. *BMC Genomics* 2013;14:381.
83. Hou J, Ma T, Cao H, Chen Y, Wang C, Chen X, *et al.* TNF-α-induced NF-κB activation promotes myofibroblast differentiation of LR-MSCs and exacerbates bleomycin-induced pulmonary fibrosis. *J Cell Physiol* 2018;233:2409–2419.
84. Tian B, Patrikeev I, Ochoa L, Vargas G, Belanger KK, Litvinov J, *et al.* NF-κB mediates mesenchymal transition, remodeling, and pulmonary fibrosis in response to chronic inflammation by viral RNA patterns. *Am J Respir Cell Mol Biol* 2017;56:506–520.
85. Beach TA, Groves AM, Williams JP, Finkelstein JN. Modeling radiation-induced lung injury: lessons learned from whole thorax irradiation. *Int J Radiat Biol* 2020;96:129–144.